Chapter 2

UHV Room Temperature Scanning Tunneling Microscope

Introduction

Since the invention of the scanning tunnelling microscope (STM) by G. Binnig and H. Rohrer [1] many different types of setups have been realized. Thereby it is necessary to (1) approach the microscopes' tip coarsely onto the sample surface until the tunnelling current sets in (typically 7 – 10 Å) and then (2) to move the tip laterally during the scanning movement over the surface. Desireable is a simple setup which combines both functions and has a sufficient stability. Successful and widespread types are e.g. the linear-motor type [2] and the Besocke beetle type [3, 4]. The latter one is named after its inventor and enables the scanners' tip to be positioned laterally and vertically on the mm scale. The speed and the resolution of a scanner are limited by its mechanical resonances which are triggered by external noise sources, thermal activation and the feed-back loop. Thereby one needs to distinguish between low-frequency noise in the range of a few Hz caused typically by intrinsic vibrations of buildings and air ventilation, and high-frequency noise caused by electronic noise and the triggered mechanical resonances. Both noise sources can be effectively reduced with an optimized scanner setup as will be presented here. Furthermore the quality of STM images and the applicability of the STM for spectroscopy and manipulation purposes relies upon the time-dependent response of the used piezo ceramics resulting in creep, hysteresis and thermal drift which will be characterized as well.

Coarse approach

All of the following scanners are based on the 10 years tradition of home-built STMs in our group [5-7] and are using a variant of the original Besocke beetle type shown in *Fig.1*. The microscope is suspended by three springs, its oscillations are damped by an eddy current damping (*Fig.2, Fig.3*). The supporting springs act as an effective damping mechanism for acoustic noise while the UHV chamber is decoupled mechanically from the ground by

damped air springs to mainly prevent low-frequency noise (*Fig.4*). Three scanners were assembled using different types and differently dimensioned piezoceramics (*Fig.1*). For the scanner 1 and scanner 2 operated at low temperature (4 K) tube piezos of different length and thickness were used. In the latest optimized setup for the operation at room temperature (scanner 3) shear stack piezoelectric elements were used.

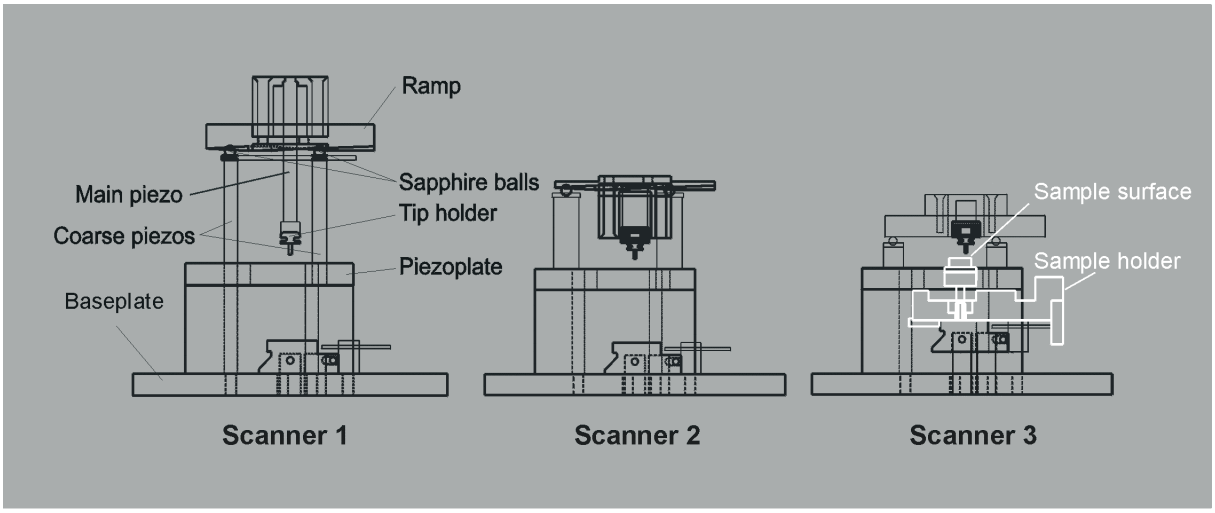

Fig.1

Side view of the three described scanners with differently dimensioned and different types of piezo ceramics. From left to right the mechanical resonance frequencies increase. Additionally the overall height decreases, making the scanner less sensitive to low-frequency noise.

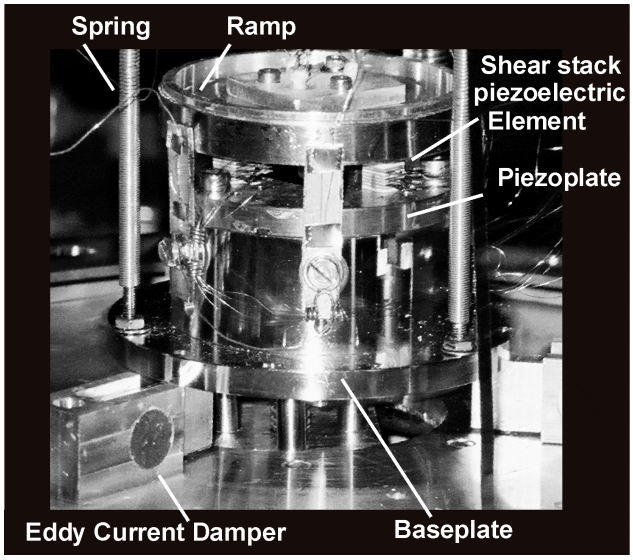

Fig.2

A photography of the scanner with the shear stack piezoelectric elements.

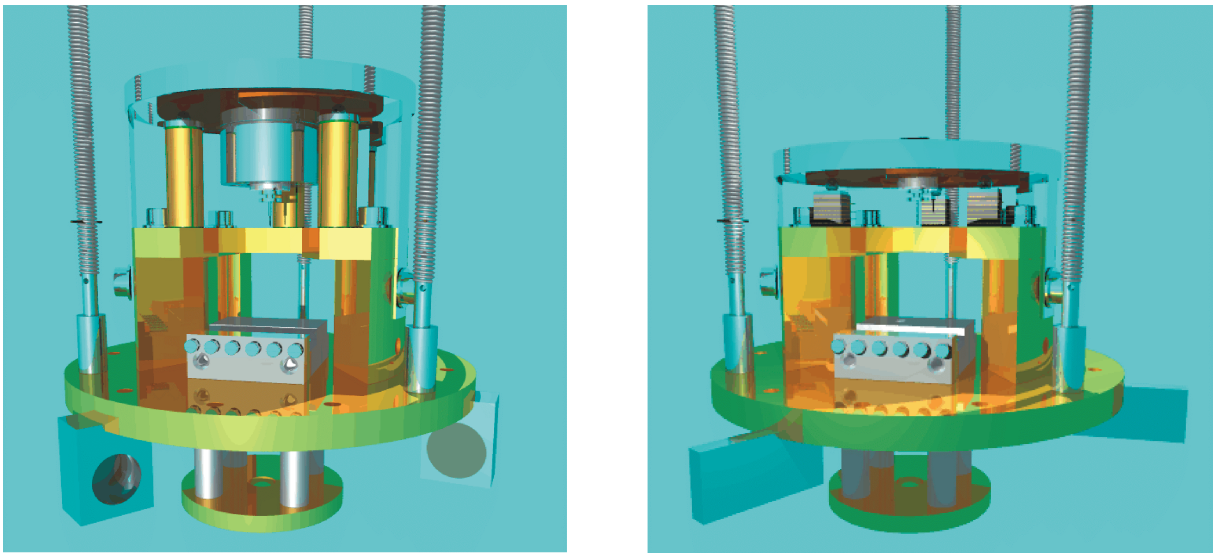

Fig.3

A detailed comparison of a scanner with the tube piezos (scanner 2) and a scanner with shear stack piezoelectric elements.

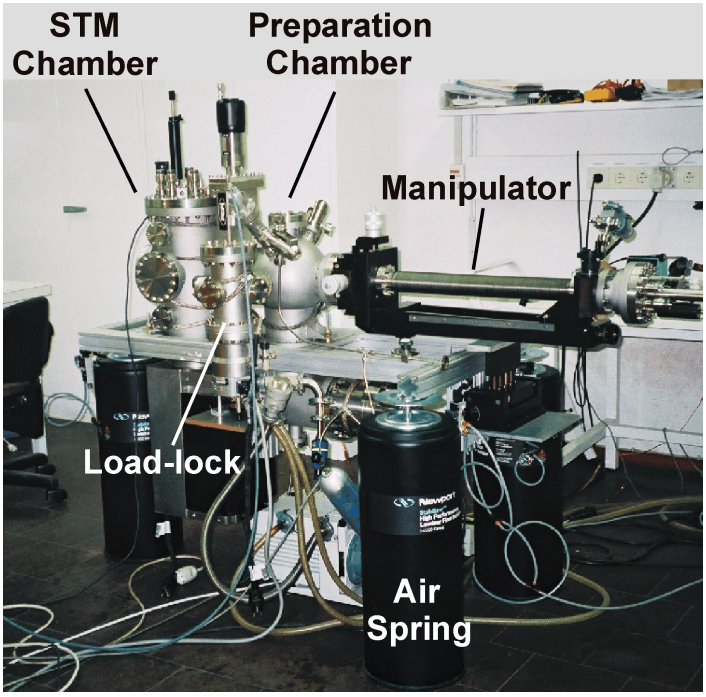

Fig.4

Picture of the UHV chamber system for the room temperature STM. The setup consists of main (STM) and preparation chambers separated by a valve, load lock and manipulator. The setup is mounted on three damped air springs.

The coarse approach is achieved in a stick-slip motion of the three outer piezo ceramics resulting in a rotation of the supported disc. The tilted ramp profile (here 2°) of the disc results then in an approach/withdrawal of the attached tip. A minimum amplitude is required for the rotational movement. The downward rotation is facilitated by gravitational forces, therefore the upwards movement is the critical direction. For the stick-slip movement usually a saw-tooth like voltage profile is applied to the piezoceramics. Experiments have shown that a parabolic profile is more effective using the maximum adhesive force for a constant acceleration throughout the whole profile. Too small amplitudes did not move the ramp whereas too high frequencies let the ramp slide around in an uncontrolled manner. Amplitude and frequency can be chosen within these limits as long as the maximum possible speed is not exceeded.

The ramp is moving on sapphire balls (*Fig.1*), where polished and unpolished sapphire balls showed equal performance. For the ramp disc Cu or Al was used. The supporting sapphire balls leave traces in both of these softer materials but only in case of Al a degradation of the performance after several years was observed. The surface of the ramp disc is polished with diamond paste of 3 μm grain size, a grain size of 1 μm resulted in too low adhesive friction. A recent ramp disc used together with shear piezos showed excellent performance although the surface was only milled. We therefore conclude that the sliding and adhesive friction enter as parameters in the stick-slip movement. They are determined by the mass and the moment of inertia of the ramp disc, the surface roughness, the surface material, and the stiffness of the piezos giving the time dependent response of the piezo ceramics.

Noise reduction and vibrational characterization

One of the ways to make the setup more stable is to make it smaller. In *Fig.1* one can find the comparison between the different STM scanner setups. From left to right a reduction of the resonance frequencies has been achieved which will be explained now.

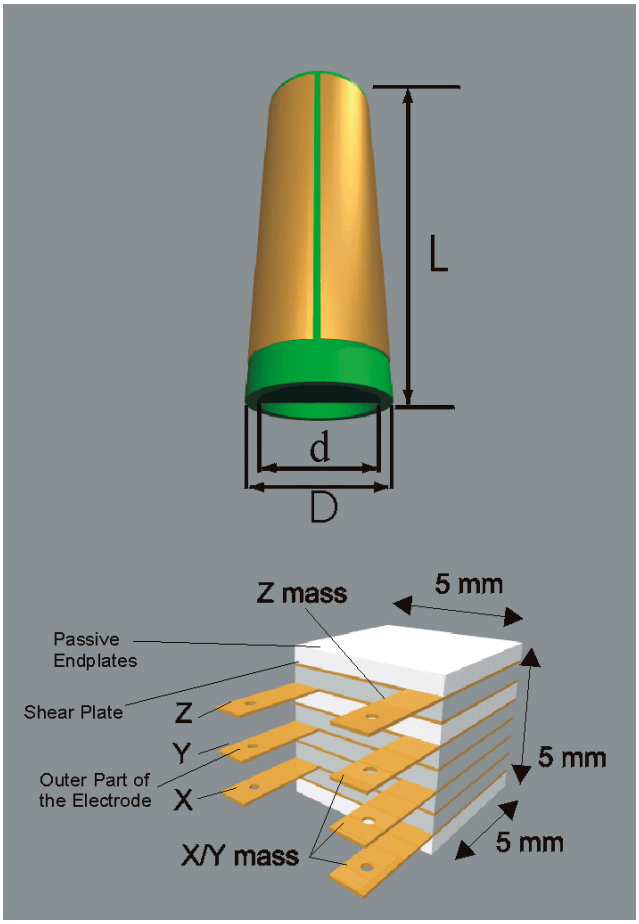

Fig.5

Design of the piezoelectric elements used in the scanners. a) Tube piezo with four segmented outer and one inner electrodes and b) shear stack piezoelement combined for a three-dimensional movement.

As mentioned above one boundary condition limits the miniaturization of the setup. A minimum amplitude of about 1.6 μm is necessary for the upward rotation of the ramp disc as determined at low temperature (4 K). This limit depends on the specific mechanical interface between the supporting sapphire balls mounted on the piezoceramics and the moving ramp disc and also on the temperature. Tube piezos were used in scanner 1 and 2 whereas in scanner 3 the shear stack piezos were used. The boundary condition was taken into account in the scanners 2 and 3. For a stable STM operation it is desireable to have the highest resonance frequencies possible.

In scanner 1 tube piezos [17] (*Fig.5*) were used and the first resonance was found to be at 300 Hz (*Fig.6*).

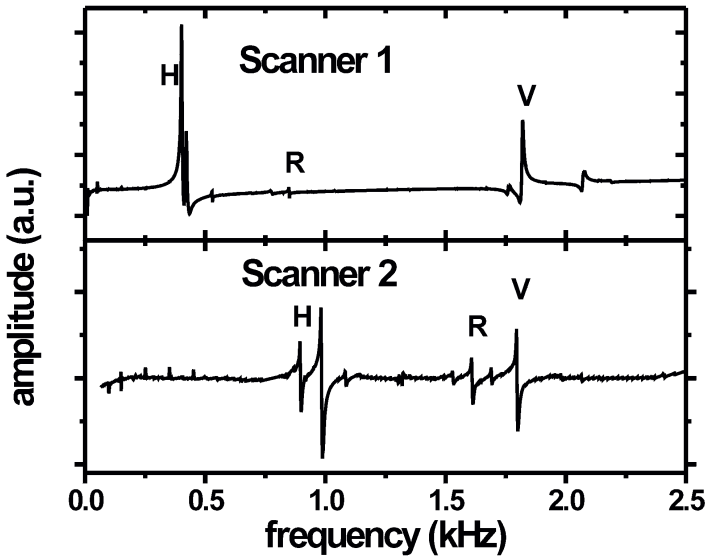

Fig.6

The vibrational response of scanner 1 and 2. The indicated labels correspond to H a horizontal, V a vertical and R a rotational mode.

The vibrational spectra were measured by exciting the bending mode of the scanner with a sinusoidal waveform (mV range) and measuring the in-phase piezoelectric voltage on other legs with a lock-in amplifier. By using different electrode configurations all of the lowest vibrational modes of the scanner could be identified: H denotes a bending mode, R a rotational mode and V a vertical oscillation. In scanner 1 the lowest measured frequencies are in accordance with calculated resonance frequencies [8]. The lowest mode can be assigned to a horizontal bending vibration, according to

$$f_H \propto \sqrt{\left(D^4 - d^4\right)/L^3 M} \propto \sqrt{\left(D/L\right)^3} \qquad (1)$$

Here M is the mass of the ramp disc (M = 22 g, Al); the other quantities are as illustrated in *Fig.5*. These resonances were found to be almost independent of temperature whereas the piezo deflection is reduced by a factor of 5 upon cooling from room temperature to liquid helium temperature. The deflection scales as [9]

$$\Delta x \propto UL^2/\left(\left(D+d\right)\left(D-d\right)\right) \propto L^2/D \qquad (2)$$

Here U is the applied voltage. It can be seen from (2) that the amplitude scales with L^2/D but the resonance frequency with $\left(D/L\right)^{3/2}$ (1). Therefore one can choose the length L or the diameter D freely and the other parameter is given by constant L^2/D. By doing so the same image size is kept but the resonances are shifted to higher frequencies. From scanner 1 to scanner 2 the piezo diameter was doubled [18] while the piezo length was reduced by a factor 0.7. The image size was reduced here to the previously determined limit.

At the same time the mass of the ramp disc was minimized to 14 g. As a result the lowest measured resonance frequency shifted up to 900 Hz (*Fig.6*). Here a lowest resonance frequency of 1.9 kHz is expected theoretically. The used formula has given values in reasonable agreement with measured values for scanners of even much less weight [8]. Therefore we have to attribute this deviation to a much lower elastic modulus than given by the manufacturer. Finally the decrease in overall height of the scanner setup resulted additionally in a reduction of low frequency noise. Forces from a torsional oscillation of the whole scanner are reduced as the torque acting on the ramp disc becomes smaller.

As apparent from (1) a decrease of the mass of the ramp e.g. by using Al as ramp material, shifts the resonance frequencies up. This approach is limited as the contact forces between the supporting sapphire balls and the ramp disc become weaker, introducing additional resonances, the so called rattling modes [8, 10, 11]. These rattling modes were not observed in the measurements presented here, possibly due to a much lower excitation amplitude and a higher ramp mass [10].

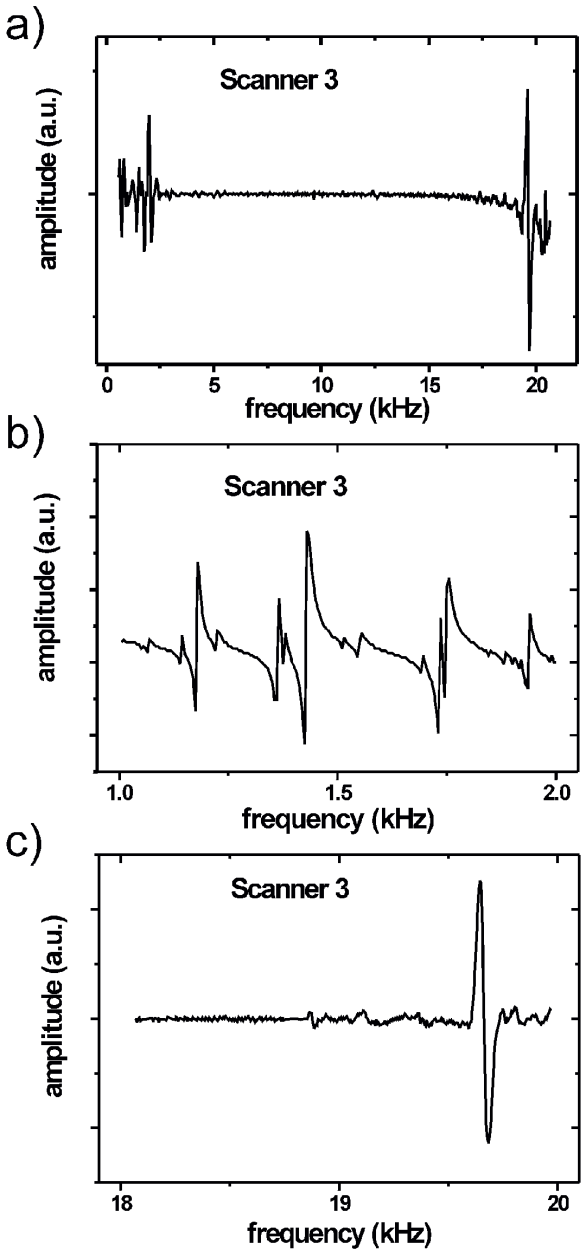

Fig.7

The vibrational response of scanner 3. The resonances between 1 and 2 kHz shown in a) and b) are present with and without ramp disc and are attributed to the contact electrodes. The resonances around 20 kHz in a) and c) scan can be assigned to a vibrational mode of the scanner.

In scanner 3 a different type of piezos was used, the shear stack piezoelements (*Fig.5*). For an explanation of the shear effect basics see Addition 1. These very stable and compact piezos allow much higher resonance frequencies and a further reduction of the overall height of the

scanner. The inverse piezoelectric shear effect results in a motion perpendicular to the applied electric field and is used here for the x and y directions. Such piezoelements became recently commercially available (PI ceramics, Germany). These actuators consist of a variable number of single shear plates and metal electrodes stacked and glued together. They can be combined for single directional or multi-directional displacement. The design of the shear piezoelectric element which is used in our experiment is shown in *Fig.5*. A normal inverse piezoeffect is used in z direction. Typical voltages needed for stick-slip upward rotation are in the order of 100V and the maximum image size amounts to (300×300) nm.

Here a very heavy ramp disc (135g, Cu) is used to avoid the rattling modes. The large mass additionally makes the scanner insensitive to external noise sources and the wiring since more energy is required for a substantial vibrational amplitude. Vibrational measurements are shown in *Fig.7*. They reveal several resonances between 1 and 2 kHz and around 20 kHz. The resonances between 1 and 2 kHz are present also without the ramp disc and can therefore be assigned to the contact electrodes. Vibrational measurements with ramp disc at higher frequencies show resonances around 20 kHz which can be estimated in the following way:

$$f = 1/2\pi\sqrt{3k/m} \tag{3}$$

Here m is the ramp mass and the factor three accounts for the number of piezos. The force constant $k = E \cdot L$ can be calculated for a cube of length L using an elastic modulus $E = 6.3 \cdot 10^{10}$ N/m. This gives a resonance frequency of 13.3 kHz for vertical and horizontal vibrational modes whereas the rotational resonance is always higher [8]. The resonances between 1 and 2 kHz do not affect the performance e.g. the feed-back loop can be operated at two orders of magnitude higher speed as compared to scanners 1 and 2. This is attributed to the mechanical stiffness of the piezos and the high ramp mass. The amplitudes of the spectra of *Fig. 6* and *7* cannot be compared directly as the different piezos required other lock-in amplifier settings. As the amplitude at the resonance scales with $1/\sqrt{k}$, a drastic reduction of the amplitude is expected dominating here over the counteracting increase of the mass.

Performance

First test measurements of the scanner 3 were done in ambient conditions with a HOPG sample. Atomic resolution (triangular and honeycomb arrangements of graphite atoms) was routinely achieved during the experiments (see Addition 2). Measurements in UHV were done with a home designed chamber system (*Fig.4*). Load-lock, preparation chamber and STM chamber have individual pumps and are connected via valves. The whole system is mounted on damped air-springs which are activated for the measurements. The manipulator can be cooled with liquid nitrogen for sample preparation if these temperatures are needed. The UHV experiment was done on a Ag(111) single crystal sample. It was cleaned by repeated sputtering cycles with Ne^+ (2.5 kV, ≈3μA) followed by a short annealing cycle up to 1000 K.
In Fig.8 terraces with monoatomic steps are shown. In *Fig.8a* a dislocation structure was induced by touching the surface with the tip. The steps of the dislocation structure appear smooth whereas the other steps appear fringy. This fringiness is not an instrumental effect but results from a tip-induced roughening of the steps [12, 13]. In *Fig.8b* the scan direction has been chosen to be parallel to the sharp step edges which show no roughness anymore.

Fig.8

Large scale images of Ag(111) surface (a) 70x40 nm, I=1.2 nA U=+0.5 V b) 35x35 nm). One can see big flat terraces, steps and some defects (dislocations) on these images. The images are only plane subtracted and not smoothed.

During the experiment atomic resolution images of the Ag(111) surface were routinely obtained as shown in *Fig.9*. This proves stable performance of the new scanner setup at room temperature and under UHV conditions. Measured corrugation amplitudes range from 4 to 20 pm and are not expected for tunnelling with a bare metal tip. Short ranged tip-surface

interaction forces can explain enhanced corrugation amplitudes on close-packed metal surfaces [14] as well as chemically modified tips [15]. The images are only plane subtracted and not smoothed. The visible noise includes instrumental effects as well as noise arising from an instable tip state. An upper limit of the instrumental noise level of 1 pm can be estimated from these images.

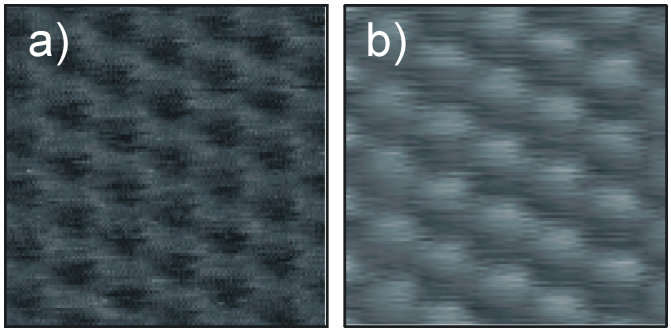

Fig.9

Atomic resolution images of the Ag(111) surface. The images are only plane subtracted and not smoothed. With the chemically modified tip a corrugation amplitude of 4 pm was measured in image a) (1.6×1.6 nm, I=11 nA U=-138 mV, tip speed 20 nm/s) and a higher value of 20 pm in image b) (1.4×1.4 nm, I=13 nA U=+149 mV, tip speed 149 nm/s) .On the right image atoms are displayed while on the left image holes are displayed. The inversion of the contrast is due to a special tip state.

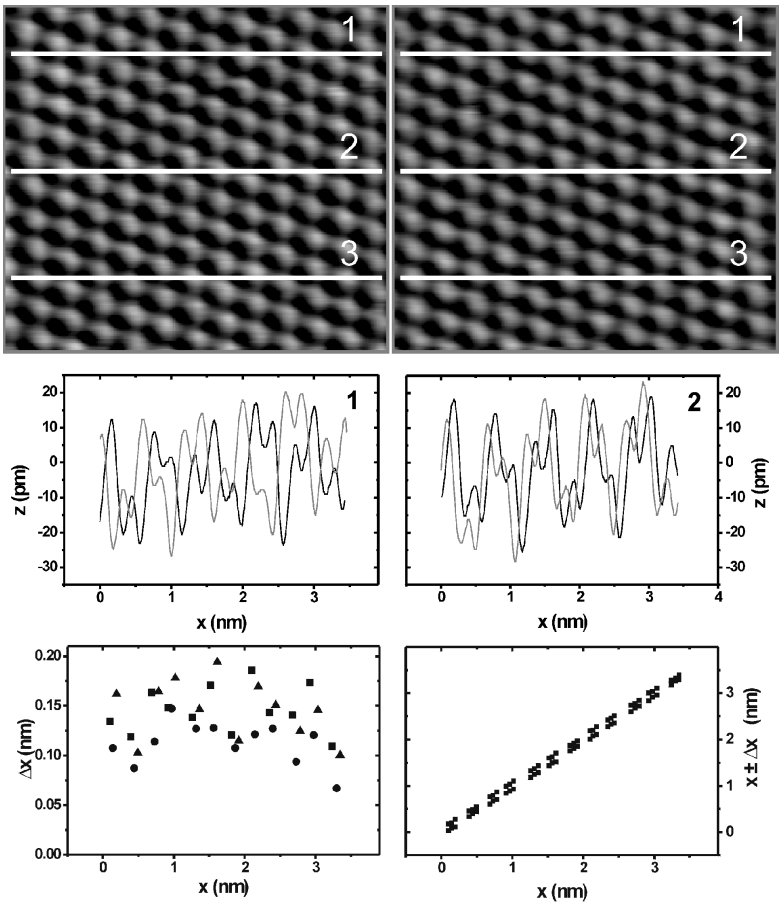

Fig.10

Atomically resolved image of the Ag(111) surface (3.4×3.4 nm, I=13 nA U=155 mV, tip speed 1700 nm/s). The left image is recorded while the tip is scanning from left to right and the right image is recorded on the backward direction. Linescans taken in the same line exhibit a displacement of the atomic positions which is shown in the lower left graph. Here the back line denotes the forward and the grey line the backward direction. The display of the displacement as a function of the mean position gives the hysteresis shown in the lower right graph.

In *Fig.10* forward and backward images of the atomically resolved Ag(111) surface are presented. Here the tip is scanning from left to right (left image) and then returns in the same line from right to left (right image). The atomic positions in one line were measured and then the difference in position between left and right image was determined. This difference as a function of the mean displacement is shown in *Fig.10* in the lower right graph and yields a hysteresis [19]. This data was taken after repeatedly scanning over the same surface area for sufficiently long time to ensure a stationary situation.

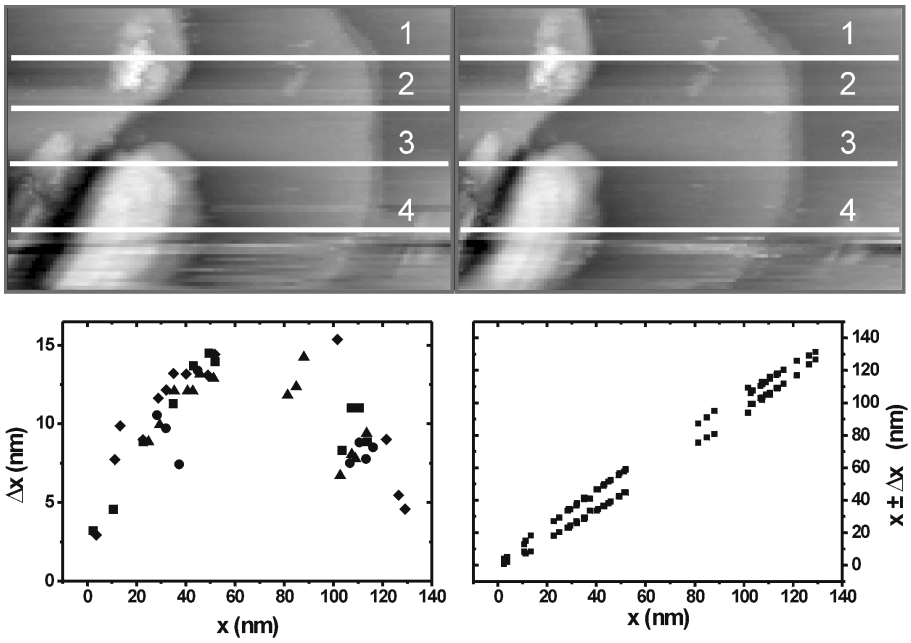

Fig.11

Same as in Fig.10 but for a lager image area (130×90 nm, I=2 nA U=0.56 V, tip speed 200 nm/s), the hysteresis has an increased loop as compared to small images.

The loop of the hysteresis depends on the image size and increases for larger images as shown in *Fig.11*. The data display a nonlinear brim followed by a constant offset. The hysteresis was found also to depend on the scanning speed (not shown here). The presented data characterizes the shear piezos under normal operating conditions, a theoretical description of the hysteresis can be found in [19]. In a microscopic picture the mechanical properties are determined by irreversible domain wall shifting pinned at defects [16]. This domain wall shifting can also be thermally activated and results in creep which is much reduced at low temperatures. Thermal drift is caused by small temperature changes of the STM. Thereby the thermal expansion of the piezos and supporting parts changes the tip position. It can be partially compensated by using the same piezo ceramics for the coarse and main position (*Fig.1*). The large diameter of the shear piezos equalizes thermal gradients rather fast which results in minor thermal drift. The values characterize a performance of the shear piezos being properly suited for the operation in a Besocke beetle type. For the measurements on the Ga (010) surface the scanner was cooled and the setup was slightly modified (see Chapter 4, RT STM measurements section).

Conclusion

Although a variety of STM scanner types have been developed since the rise of the STM, approaches to improve the stability of the most common type i.e. the Besocke-beetle type are sparse. The instrumental setup and thorough optimization of a STM for the operation at room temperature was a major part of the present work. Both low-frequency and high-frequency noise sources were effectively reduced with an optimized Besocke-beetle scanner setup. This scanner setup was optimized for the operation at room temperature by using for the first time a new type of the piezoelectric elements – shear stack piezoelectric elements. This resulted in very high resonance frequencies and overall stability - the resonance frequencies were improved by more than one order of magnitude as compared to commonly used tube piezos. This scanner was then implemented in a home designed UHV system, the setup of this UHV system was also part of the present work.

References

[1] G. Binnig and H. Rohrer, Helv. Phys. Acta **55**, 726 (1982).

[2] S.H. Pan, E.W. Hudson, and J.C. Davies, Rev. Sci. Instr. **70**, 1459 (1999).

[3] K. Besocke, Surf. Sci. **181**,145 (1987).

[4] J. Frohn, J. Wolf, K. Besocke, and M. Teske, Rev. Sci. Instr. **60**, 1200 (1989).

[5] G. Meyer, Rev. Sci. Instr. **67**, 2960 (1996).

[6] K.-F. Braun, Ph.D. thesis, Freie Universität Berlin, 2001.

[7] S. Zöphel, Ph.D. thesis, Freie Universität Berlin, 2000.

[8] S. Behler, M.K. Rose, D.F. Ogletree, and M. Salmeron, Rev. Sci. Instr. **68**, 124 (1997).

[9] C.J. Chen, Appl. Phys. **60**, 132 (1992).

[10] J.M. MacLeod, A. Moffat, J.A. Miwa, A.G. Mark, G.K. Mullins, R.H.J. Dumont, G.E. Contant, and A.B. McLean, Rev. Sci. Instr. **74**, 2429 (2003).

[11] J.A. Miwa, J.M. MacLeod, A. Moffat, and A.B. McLean, Ultramicroscopy, in press (2003).

[12] J.J. Schulz, R. Koch, and K.H. Rieder, Phys. Rev. Lett. **84**, 4597 (2000).

[13] R. Koch, J.J. Schulz, Phys. Rev. Lett. **87**, 039604 (2001).

[14] W.A. Hofer, A.J. Fisher, R.A. Wolkow, and P.Grütter, Phys. Rev. Lett. **87**, 236104 (2001).

[15] B. Neu, G. Meyer, and K.-H. Rieder, Mod. Phys. Lett. B **9**, 963 (1995).

[16] J. Roedel, W.S. Kreher, Proceedings of SPIE, **4333** (2001).

[17] Staveley Sensors EBL#2: L=25.4 mm D=3.2 mm W=0.5mm

[18] Staveley Sensors EBL#2: L=18.5 mm D=6.5 mm W=0.5mm

[19] K. Dirscherl, J. Garnaes, L. Nielsen, J. Vac. Sci. & Techn. B, **18**, 621 (2000).